


## Article

# Improvement of Heat Dissipation Characteristics of Cu Bus-Bar in the Switchboards through Shape Modification and Surface Treatment

Min-Jun Kim <sup>1</sup>, Sang-Hwan Bak <sup>1</sup>, Woo-Chul Jung <sup>1</sup>, Deog-Jae Hur <sup>2</sup> , Dong-Shin Ko <sup>2</sup> and Man-Sik Kong <sup>1,\*</sup>

<sup>1</sup> Advanced Materials & Processing Center, Institute for Advanced Engineering (IAE), Yongin 175-28, Korea; minjun@iae.re.kr (M.-J.K.); shbak@iae.re.kr (S.-H.B.); dncjf7513@iae.re.kr (W.-C.J.)

<sup>2</sup> Research & Business Cooperation Center, Institute for Advanced Engineering (IAE), Yongin 175-28, Korea; djhur@iae.re.kr (D.-J.H.); dsko@iae.re.kr (D.-S.K.)

\* Correspondence: mskong@iae.re.kr; Tel.: +82-31-330-7480

Received: 21 November 2018; Accepted: 27 December 2018; Published: 2 January 2019



**Abstract:** In order to improve energy efficiency by increasing heat dissipation performance of bus-bar which distributes the current in high-power switchboard, the heat dissipation effects of the shape modification and surface treatment of Cu bus-bar were studied. The surface temperatures of the conventional plate-type bus-bar, and the improved tunnel-type bus-bar were compared by using electromagnetic and thermal analyses. The optimum thickness of tunnel-type bus-bar and the spacing and array among three bus-bars were calculated; and the surface temperature of tunnel-type bus-bar showed 7.9 °C lower than that of plate-type bus-bar in a 3-phase array condition. In addition, the surface and internal temperatures of the uncoated, CNT (Carbon nanotube)-coated, and BN (Boron nitride)-coated Cu bus-bars were measured with thermal imaging camera and the experiment using a hot plate. It was confirmed that the difference in the internal temperature between uncoated and BN-coated Cu was 19.4 °C. The application of the bus-bar improved from this study might contribute to the increase in power energy efficiency.

**Keywords:** switchboard system; Cu bus-bar; heat dissipation; electromagnetic thermal analysis; boron nitride coating

## 1. Introduction

The switchboard is a device that distributes power supplied from the power company or the power plant with each circuit breaker by electrically connecting them to the appropriate power source according to the rating of various facilities and equipment actually used. In order to distribute the power, the switchboard supplies power to various facilities through the main circuit breaker installed in a panel or a frame and a bus-bar connected to a plurality of branch circuit breakers, while simultaneously performing a function of opening and closing the power supply. Bus-bar, which is mainly made of copper and aluminum, is a conductor used in place of the power cable. It is mainly used in high-power switchboards because it has a higher heat dissipation effect than cables and it also has a larger surface area to lower the impedance of the high-frequency current flowing on the surface of the conductor. The bus-bars are divided into a rectangular plate structure and a circular concentric pipe structure, depending on the shape [1–3]. When the bus-bar is connected to the terminal in the switchboard, the connection part with the terminal is subjected to additional processing such as hole machining or flat forming. The size of the switchboard is becoming larger as the demand for stabilized power increases, making the assembly process more complex [4]. In order to resolve the problem of power efficiency and current density degradation due to the heat generated by electromagnetic

interference among bus-bars in the switchboard, an approach to shaping design of the bus-bar is required to improve the cooling efficiency. In addition, since the increase in size of the bus-bar is inevitable due to the increase in the demand for the stable power, the volume and the weight of the switchboard also increases depending on the size of the bus-bar, so the shape and the arrangement of the bus-bar in the switchboard are important [5–8].

In the case of a plate-shaped bus-bar arranged parallel to the inside of the switchboard, if the current flows in a certain direction, the attraction and the repulsive forces are generated due to the influence of the electromagnetic field formed around the conductor. At this time, because the plate surface area facing each other is relatively large, the bus-bar is not stabilized due to the influence of the electromagnetic field. The bus-bar cannot bend in the three-axis direction when the bus-bar is placed in the switchboard, hence, the volume of the switchboard increases.

Cylindrical bus-bar was developed to resolve the problems of plate-shaped bus-bars, and they can reduce the interference of electromagnetic fields from adjacent bus-bars while occupying a relatively small volume [9,10].

However, in the same manner as the plate-shaped bus-bar, the electric resistance characteristic of the cylindrical bus-bar is changed due to the deformation of the joint parts by the pressing process during the fastening of the bus-bar. In addition, the current path of the joint parts is changed due to the screw, resulting in a localized temperature rise. Moreover, it is important to simplify the design of the bus-bar joint for minimizing the power loss by the heat generation and the mechanical stiffness degradation of the machined part caused by the pressing process for connecting the bus-bar and the terminal [11,12].

Eddy current, which is caused due to electromagnetic field, increases the resistance of the conductor and it can decrease the energy efficiency. By applying the technology to suppress or shield the eddy current, it is possible to suppress the rise of the conductor resistance from the electromagnetic field and improve energy efficiency [13]. To shield the vortex generated by the bus-bars in the switchboard, it is possible to reduce the power loss by suppressing the temperature rise by minimizing the occurrence of vortices by adopting a material which can shield or absorb the electromagnetic wave instead of the existing material.

There are several studies to solve the problems related to electromagnetic field [14–18], thermal field [19], temperature distribution over the surface of bus-bars [20], connection and bus-bar joint resistance [21–23] in the bus-bar system. However, it is important to verify quantitative actual bus-bar temperature, not only the electromagnetic and thermal analyses, but also the measurements of bus-bar temperature with the various positions.

In this study, the development of the improved bus-bar indicating high heat dissipation performance and power efficiency compared to the conventional bus-bar was performed; and the optimal bus-bar model was proposed based on the results of the electromagnetic field analysis according to the shape of the bus-bar and surface treatment technique to improve the heat dissipation characteristics of the bus-bar itself.

## 2. Experimental Procedures

### 2.1. Electromagnetic and Thermal Analysis Conditions of the Bus-Bar

In this study, copper was used as the bus-bar material, and its analyses for electromagnetic and thermal properties were performed. The air field area was utilized to analyze the electromagnetic and thermal characteristics at room temperature of 25 °C. Table 1 shows the density, thermal conductivity, specific heat, electric conductivity and magnetic permeability of copper, and air used for electromagnetic and thermal analyses.

**Table 1.** Properties of copper and air for electromagnetic and thermal analyses.

Material	Density (kg/m <sup>3</sup> )	Thermal Conductivity (W/m·K)	Specific Heat (J/kg·K)	Electric Conductivity (S/m)	Magnetic Permeability (H/m)
Copper	8960	401	385	$5.81 \times 10^7$	$1.256 \times 10^{-6}$
Air	1.205	0.0257	1005	$3.00 \times 10^{-15}$	$1.256 \times 10^{-6}$

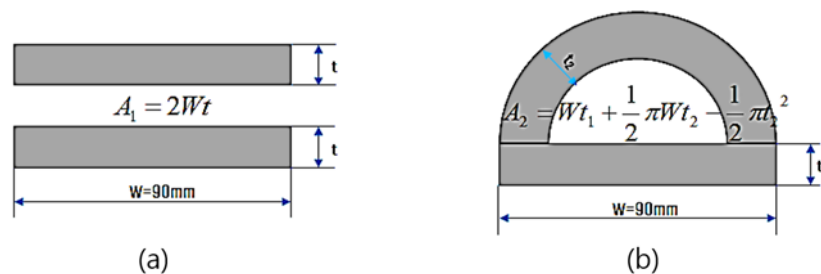
In order to compare the electromagnetic and thermal characteristics of plate-type bus-bar with tunnel-type bus-bar, the alternating current of 3000 A<sub>rms</sub> and 60 Hz were applied to bus-bar. The electromagnetic field analysis was based on a time harmonic processor, and the heat transfer analysis was based on a transient processor. In the case of boundary condition, Robin boundary condition, which combined Dirichlet boundary condition that defines  $V = 0$  along the boundary to maintain the magnetic flux with Neumann boundary condition that forcibly defines the magnetic flux passing through the boundary at 90-degree angle, was applied. In addition, convection heat transfer coefficient of 6 W/m<sup>2</sup>·K at the room temperature was applied to consider the effect of natural convection of air. ABAQUS program (2017 Standard, Dassault System, Vélizy-Villacoublay, France) was used for simulation analysis in this study.

In order to develop a bus-bar design indicating optimal heat dissipation characteristics, the case study for the cross-sectional shapes of tunnel-type bus-bar was performed. The cross-sections of plate-type and tunnel-type bus-bars are shown in Figure 1, and the cross-sectional areas are calculated using Equations (1) and (2).

$$A_1 = 2Wt \quad (1)$$

$$A_2 = Wt_1 + \frac{1}{2}\pi Wt_2^2 - \frac{1}{2}\pi t_2^2 \quad (2)$$

where  $A_1$  and  $A_2$  are cross sectional areas of the plate-type and tunnel-type bus-bar respectively,  $W$  is the width of bus-bar which define as 90 mm,  $t$  is the thickness of plate-type bus-bar,  $t_1$  is the thickness of plate part of tunnel-type bus-bar, and  $t_2$  is the thickness of semi-pipe part of tunnel-type bus-bar.

**Figure 1.** Schematics of cross-sections of bus-bar; (a) Plate-type, (b) Tunnel-type.

At first, the case study for the thickness of tunnel-type bus-bar is calculated with the condition that both the cross-sectional areas of plate-type and tunnel-type are equal. An equivalent condition for cross-sectional areas of the plate-type and tunnel-type bus-bars can be summarized as Equation (3).

$$2Wt = Wt_1 + \frac{1}{2}\pi Wt_2^2 - \frac{1}{2}\pi t_2^2 \quad (3)$$

In order to obtain the  $t_1$  and  $t_2$  values, the following Equation (3) can be expressed as a quadratic Equation (4).

$$\pi t_2^2 - \pi Wt_2 + 4Wt - 2Wt_1 = 0 \quad (4)$$

Equation (4) can be summarized as Equation (5) by applying the formula of the quadratic equation.

$$t_2 = \frac{\pi W \pm \sqrt{(\pi W)^2 - 4\pi(4Wt - 2Wt_1)}}{2\pi} \quad (5)$$

Table 2 shows  $t_1$  and  $t_2$  of the tunnel-type bus-bar having the same cross-sectional area with the plate-type bus-bar when  $t$  is 10 mm.

**Table 2.** Case studies of the  $t_1$  and  $t_2$  values of the tunnel-type bus-bar satisfying area of 1800 mm<sup>2</sup>.

Case	$t_1$ (mm)	$t_2$ (mm)	Cross-Sectional Area (mm <sup>2</sup> )
1	9.0	7.65	1800
2	10.0	6.89	
3	11.0	6.15	
4	12.0	5.42	

## 2.2. Evaluation of Properties of Coating for Heat Dissipation

In order to improve the heat release rate of the distribution system, the applicability of two coating materials that are CNT (Carbon nanotube) based material and BN (Boron nitride) based material on the bus-bar were investigated. The copper substrate specimens that are  $30 \times 30 \times 10$  mm<sup>3</sup> were prepared and two coating materials were coated on the substrates respectively. The thickness of the coated materials on the substrates measured with SEM (Scanning electron microscopy) was about 70  $\mu$ m. The emissivity and radiation energy were measured at the temperature of 50 °C and 80 °C by using FT-IR (Fourier transform infrared) spectrometer (WQF-510A, Rayleigh, Beijing, China).

To investigate the heat dissipation effect of coating materials, the temperatures of the surface of three specimens (Uncoated Cu, CNT-coated Cu, and BN-coated Cu) were measured with thermal imaging camera (M2400-C, MIDAC, Westfield, MA, USA). The size of the copper substrates was  $50 \times 50 \times 10$  mm<sup>3</sup> and the surface temperatures of the specimens were measured after 1 h exposure duration at atmosphere temperatures of 50 °C and 80 °C.

To measure the temperatures of internal Cu of the three specimens, thermocouples were inserted into Cu substrate and temperature rise test was performed by using a hot plate. The underside plane of Cu substrate attached with a hot plate was not coated and the opposite plane was coated in this experiment. Figure 2 shows the schematic of the experiment for measurement of internal temperature of the Cu substrate. Setting temperature range was 50~300 °C and the internal temperature of the Cu substrate was measured after 30 min after setting the target temperature.

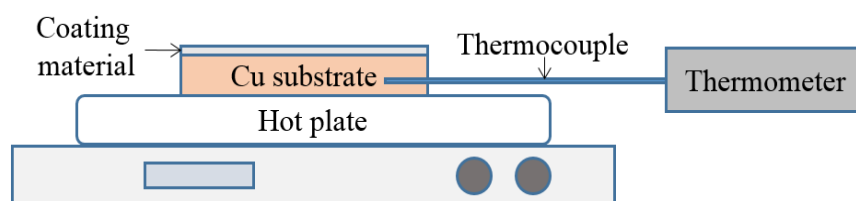
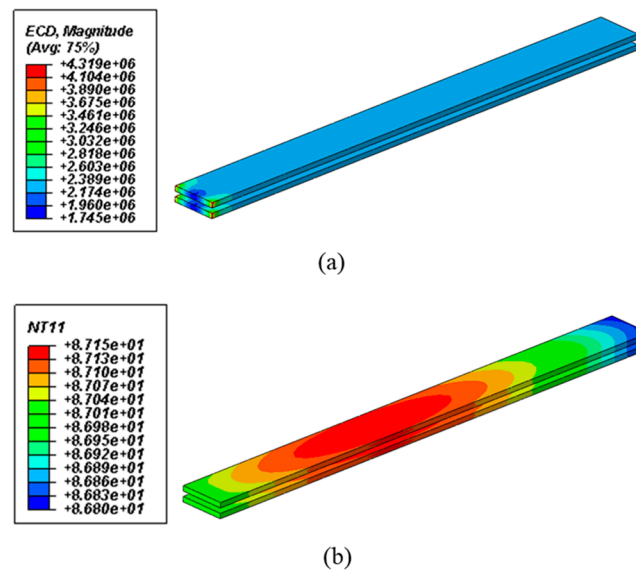


**Figure 2.** Schematic of the experiment for measurement of internal temperature of Cu substrate using a hot plate.

## 3. Results and Discussion

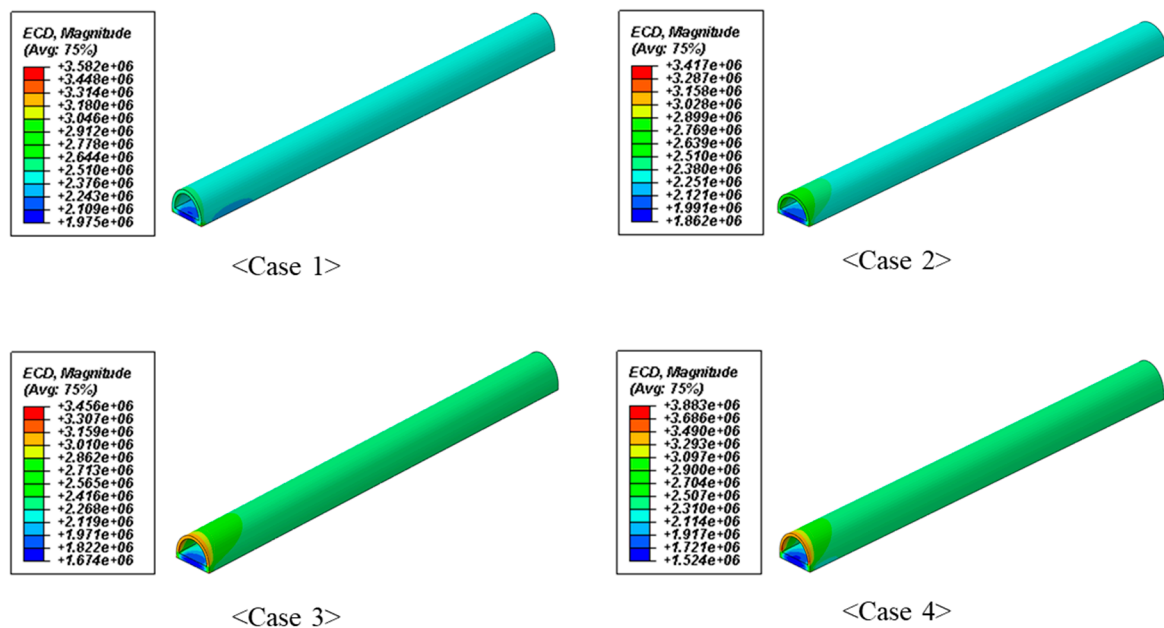
### 3.1. Electromagnetic and Thermal Analysis for Shape of Bus-Bar

Figure 3 shows the electromagnetic and thermal analysis for plate-type bus-bar. The current density distribution in plate-type bus-bar was uniform and the temperature by exothermic reaction at the center of the bus-bar was raised up to 87.1 °C. The difference of maximum and minimum temperatures of plate-type bus-bar was 0.34 °C.



**Figure 3.** Results of the electromagnetic and thermal analysis for plate-type bus-bar: (a) Current density; (b) thermal gradient.

Figure 4 shows the results of the current density analysis in tunnel-type bus-bar as a function of thickness. The tunnel-type bus-bars also show uniform current densities on the whole regardless of the thickness. It was confirmed that there was no position that acted as a localized resistance when the current was applied to the tunnel-type bus-bar.



**Figure 4.** Results of the current density distribution analysis as a function of the thickness of tunnel-type bus-bar.

Figure 5 shows the results of the thermal analysis in tunnel-type bus-bar as a function of thickness. The elevated temperatures due to the exothermic reaction at the center of bus-bar are shown in Table 3. The tunnel-type bus-bar which has the same sectional area with the plate-type bus-bar shows lower heat generation temperature. The tunnel-type bus-bar which showed the lowest temperature was  $8.4\text{ }^{\circ}\text{C}$  lower than the plate-type bus-bar. It was analyzed that the inner area exposed to air through the tunnel structure is advantageous for heat dissipation and the inner area exposed to air

was increased with the decrease of the thickness of semi-pipe part. Therefore, the thinner thickness of the semi-pipe part in the tunnel-type bus-bar causes more heat dissipation and lower temperature of bus-bar. Consequently, it is important to determine the semi-pipe part and plate-part thickness considering the efficiency of manufacturing.

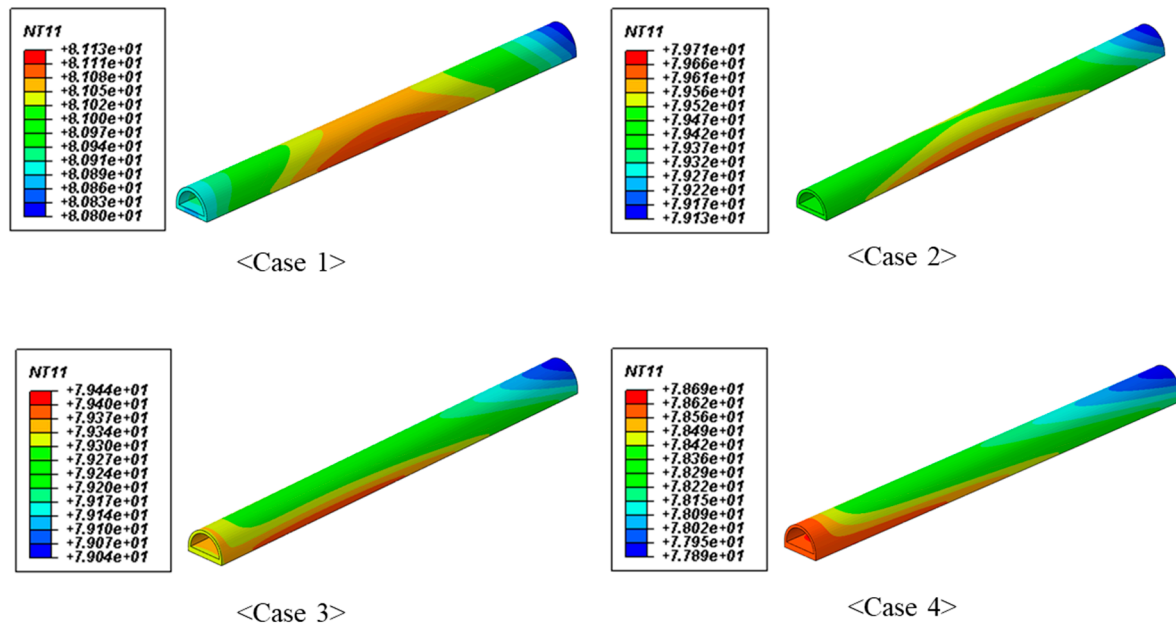


**Figure 5.** Results of the thermal distribution analysis as a function of the thickness of tunnel-type bus-bar.

**Table 3.** Elevated temperatures as a function of tunnel-type bus-bar thickness calculated from thermal analysis.

Case	1	2	3	4
Elevated temperature (°C)	81.1	79.7	79.4	78.7

To analyze the heating characteristics for the compact arrangement of bus-bars, a 3-phase parallel array analysis was carried out for the proposed design based on the optimization of the tunnel-type bus-bar shape. In a parallel array analysis, the cross-sectional area was expanded to 2000 mm<sup>2</sup>. The alternating current of 3000 A<sub>rms</sub> and 60 Hz was applied to each phase of the bus-bar with the phase difference of 120-degree. It consists of both the air field and bus-bar area to account for electromagnetic and thermal properties simultaneously. The minimum  $t_2$  value considering manufacturability was 7 mm and the spacing among the bus-bars was derived as shown in Figure 6.

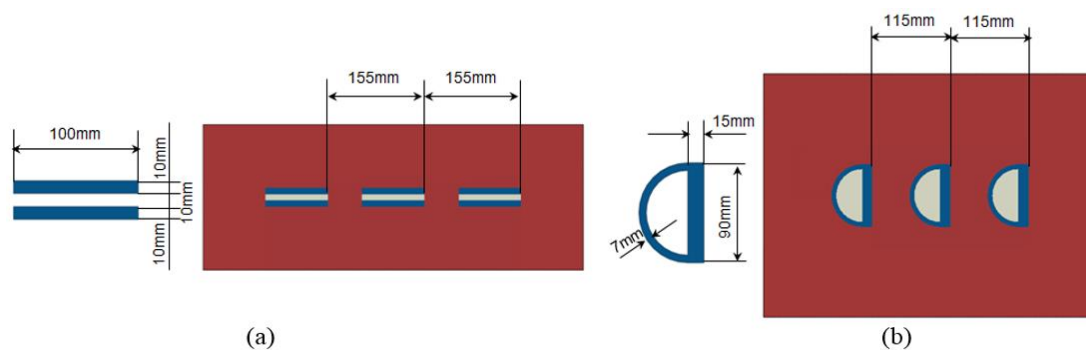


**Figure 6.** Geometry of 3-phase parallel arrays of bus-bars: (a) Plate-type, (b) Tunnel-type.



Figures 7 and 8 show the electromagnetic and thermal analysis for a 3-phase parallel array of plate-type and tunnel-type bus-bar. Among the arrayed three bus-bars, the bus-bar located in the center shows the highest temperature rise regardless of the shape of the bus-bar. The maximum temperature of plate-type is 83.1 °C which is higher than that of tunnel-type indicating 75.0 °C and it means that tunnel-type bus-bar has more effective heat dissipation characteristic than plate-type bus-bar in parallel arrayed condition. Therefore, it was confirmed that the use of tunnel-type bus-bar in switchboard could decrease the heat resistance by an advantageous structure for heat dissipation than plate-type bus-bar and it could have a positive effect on energy efficiency.

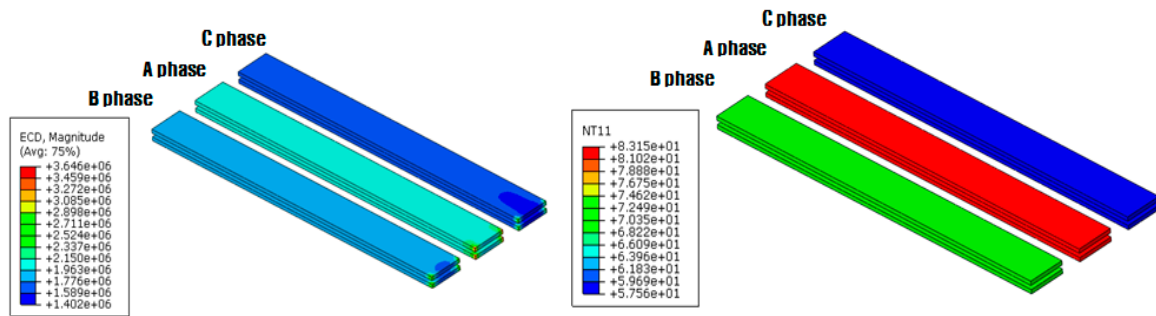


Figure 7. Electromagnetic and thermal analysis for 3-phase parallel array of plate-type bus-bar.

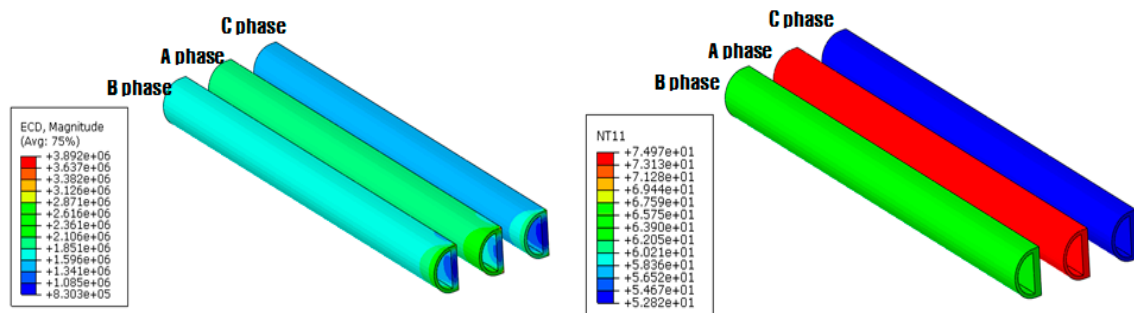


Figure 8. Electromagnetic and thermal analysis for 3-phase parallel array of tunnel-type bus-bar.

### 3.2. Heat Dissipation Characteristics of CNT and BN Coated Specimens

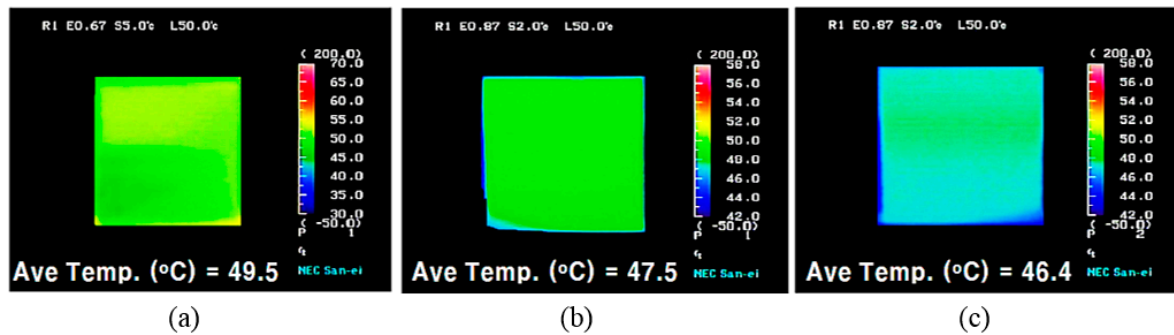
The emissivity and radiant energy of the base material and coated specimens were measured with thermal imaging camera to confirm the change in heat dissipation characteristics of the bus-bar to which the coating was applied and the results are shown in Table 4. The emissivity and radiant energy of CNT or BN coated specimens were higher than the copper substrates. Compared with two coating materials, BN-coated specimen showed the highest emissivity and radiation energy. In addition, the emissivity and radiant energy of all specimens were slightly decreased with increasing atmospheric temperature.

Table 4. Emissivity and radiation energy of uncoated and coated Cu specimens at 50 °C and 80 °C.

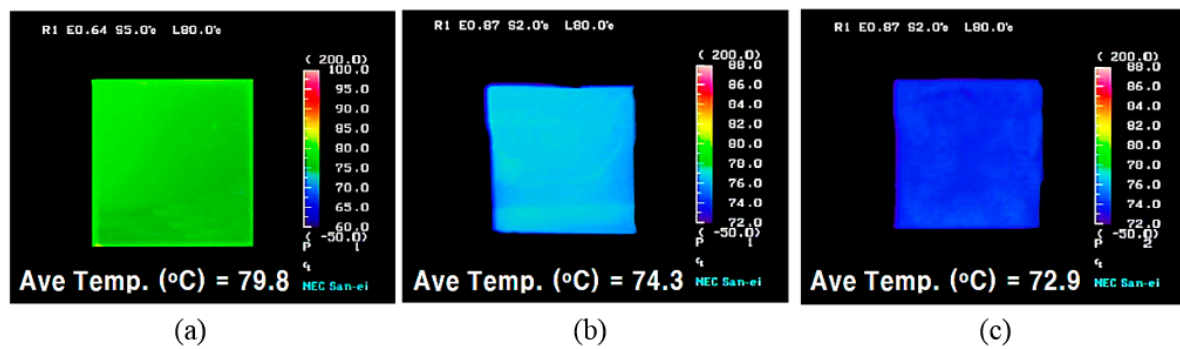
Sample	50 °C		80 °C	
	Emissivity	Radiation Energy (W/m <sup>2</sup> ·μm)	Emissivity	Radiation Energy (W/m <sup>2</sup> ·μm)
Uncoated Cu	0.535	$2.48 \times 10^2$	0.524	$3.57 \times 10^2$
CNT-coated Cu	0.872	$4.04 \times 10^2$	0.867	$5.91 \times 10^2$
BN-coated Cu	0.874	$4.05 \times 10^2$	0.868	$5.91 \times 10^2$

Figure 9 shows the images of the surface of three specimens at atmospheric temperature of 50 °C. The BN-coated specimen showed the lowest surface temperature among three specimens. The heat dissipation rates of CNT-coated Cu and BN-coated Cu for uncoated Cu calculated by average temperatures are 4.04% and 6.26% respectively. As shown in Figure 10, the results at the atmospheric

temperature of 80 °C showed similar results to the atmospheric temperature of 50 °C. The heat dissipation rates of the coated specimens at 80 °C are 6.89% and 8.65%.



**Figure 9.** Photographs of the surfaces of the specimens measured by thermal image camera at an atmosphere temperature of 50 °C: (a) Uncoated Cu, (b) CNT-coated Cu, (c) BN-coated Cu.



**Figure 10.** Photographs of the surfaces of the specimens measured by thermal image camera at an atmosphere temperature of 80 °C; (a) Uncoated Cu, (b) CNT-coated Cu, (c) BN-coated Cu.

The temperature-drop of the surface by applying coating material was confirmed by a thermal imaging camera. In order to clearly identify the temperature-drop of bus-bar due to the effect of heat dissipation, it is necessary to measure the temperature inside the bus-bar as well as the surface of the bus-bar. Figure 11 shows the internal temperatures of uncoated and coated Cu as a function of setting temperatures. Uncoated Cu specimen measured as a reference shows a similar temperature to the setting temperature of a hot plate from 50 °C to 200 °C. The internal substrate temperatures of coated specimens show a lower temperature than the setting temperature. In addition, temperature-drop rates of coated specimens increased more steeply with the increasing setting temperature. At the setting temperature of 80 °C, the internal temperatures of uncoated, CNT-coated, and BN-coated specimens are 77.5, 72.1, and 58.1 °C respectively. From the results of Figures 10 and 11, it could be inferred that the surface temperature might be higher than the internal substrate temperature in all specimens, although the difference of heating system between the atmosphere temperature control using heating chamber and the direct temperature rise at the specimens using a hot plate was present. The temperature difference of the surface and substrate of BN-coated specimen is approximately 14.8 °C, and it means that the BN coating material indicated excellent heat dissipation characteristics.



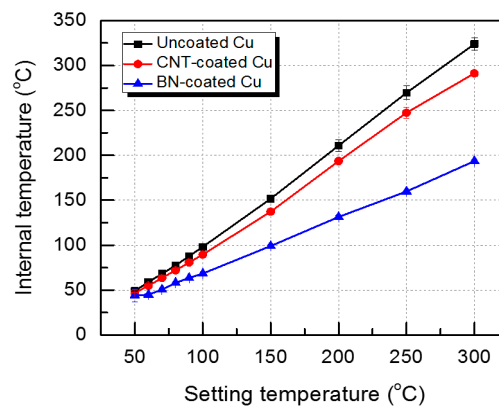


**Figure 11.** Internal temperatures of the substrates of three specimens as a function of setting temperature of a hot plate.

To verify the results of the above experiments, the temperatures of uncoated and BN-coated tunnel-type bus-bars were measured, and the schematic of the experiment and the locations of temperature-measuring sensors as shown in Figure 12. The thickness of the plate part of tunnel-type bus-bar was 10 mm and the width was 100 mm. The two bus-bars had fastened each other and 3000 A of alternating current was applied to bus-bar for 5 h. Table 5 shows the temperature rise of uncoated and BN-coated bus-bars after 5 h applying AC current. The temperature rise values were calculated by subtracting the atmosphere temperature from the measured temperature.

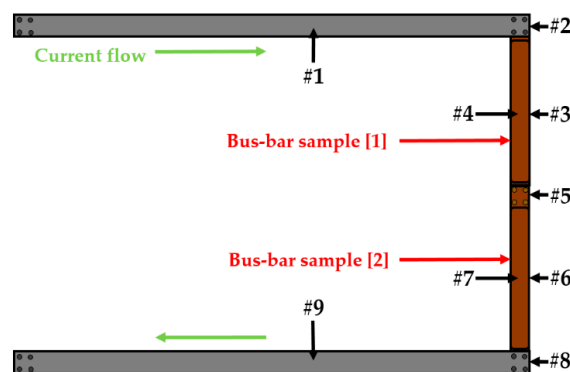


**Figure 12.** Schematic of the experiment using actual-size two tunnel-type bus-bars and the position of the temperature measuring point.

**Table 5.** Temperature rise values of plate-type, uncoated and BN-coated bus-bars.

Temperature Measuring Point	Position	Temperature Rise		
		Typical Bus-Bar	Uncoated Bus-Bar	BN-Coated Bus-Bar
		Plate-Type	Tunnel-Type	Tunnel-Type
#1	1 m front of connection part of current draw	36.2	47.3	43.4
#2	Connection part of current draw	39.4	52.5	41.6
#3	Center of sample [1] (plate part)	66.9	58.1	39.4
#4	Center of sample [1] (semi-pipe part)		58.6	38.8
#5	Connection part of sample [1] and [2]	68.1	57.9	41.9
#6	Center of sample [2] (plate part)	64.8	54.4	39.5
#7	Center of sample [2] (semi-pipe part)		54.5	39.0
#8	Connection part of current drain	58.3	47.3	38.5
#9	1 m rear of connection part of current drain	43.1	44.8	42.1

The quantitative increase of the energy efficiency by the application of the surface treatment could be calculated. The resistivity and temperature are linearly proportional as following Equation (6) [24].

$$\rho = t + 15.7 \quad (6)$$

The power,  $P$ , dissipated as heat in a bar carrying current,  $I$ , is then

$$P = S \times R_{dc} \times I^2 \quad (7)$$

$$P = S \times \frac{\rho}{A} \times I^2 \quad (8)$$

where  $P$  is the power dissipated per meter length (W/m),  $R_{dc}$  is the resistance per meter length ( $\mu\Omega/\text{m}$ ),  $S$  is shape factor,  $\rho$  is resistivity ( $\text{n}\Omega\text{m}$ ),  $A$  is cross-sectional area ( $\text{mm}^2$ ).

$P$  (W/m) is determined by resistivity at the same cross-sectional area and current condition. The rising temperatures of the typical and BN-coated bus-bar at position #4 (in Table 5) were 66.9 and 39.4 °C, respectively. From Equation (6), The resistivity of typical bus-bar was  $0.068 \times 66.9 + 15.7 = 20.2492$ , and that of BN-coated bus-bar was  $0.068 \times 39.4 + 15.7 = 18.3792$ .

Therefore, it can be calculated as Energy saving rate =  $100 \times (\text{typical bus-bar resistivity} - \text{BN coated bus-bar resistivity}) / \text{typical bus-bar resistivity} = 100 \times (20.2492 - 18.3792) / 20.2492 = 9.23\%$ .

#### 4. Conclusions

The study for the increase of energy efficiency by developing the shape of bus-bar and the surface treatment on the bus-bar was performed. Firstly, the optimal thickness of the tunnel-type bus-bar and the spacing among bus-bars in 3-phase parallel array condition were obtained by using electromagnetic and thermal analyses. The maximum surface temperature of the bus-bar developed in this study is about 8 °C lower than that of conventional plate-type bus-bar. Secondly, the temperatures of the copper substrate using CNT and BN-based coating materials were measured by using thermal imaging camera and a hot plate and it was confirmed that the BN-coated Cu had the lowest surface temperature and the temperature of substrate among three specimens. In particular, the difference of the internal temperature of uncoated Cu and BN-coated Cu by the experiment using a hot plate was 19.4 °C. It is considered that the energy loss due to heat generation in the switchboard can be reduced by applying the developed bus-bar in this study.

**Author Contributions:** Conceptualization, S.-H.B. and M.-S.K.; Methodology, S.-H.B.; Software, D.-S.K.; Validation, M.-J.K., S.-H.B. and W.-C.J.; Formal analysis, D.-S.K. and D.-J.H.; Investigation, S.-H.B.; Writing—original draft preparation, M.-J.K.; Writing—review and editing, M.-J.K., S.-H.B. and M.-S.K.

**Funding:** This work was supported by Korea Institute of Energy Technology Evaluation and Planning (KETEP) grant funded by the Korea government, MOTIE (No. 20162020107440).

**Conflicts of Interest:** The authors declare no conflict of interest.

#### References

1. Caponet, M.C.; Profumo, F.; De Doncker, R.W.; Tenconi, A. Low stray inductance bus bar design and construction for good EMC performance in power electronic circuits. *IEEE Trans. Power Electron.* **2002**, *17*, 225–231. [CrossRef]
2. Hahn, J.W.; Koch, J.K. Power Bus Bar for Providing a Low Impedance Connection between a First and Second Printed Circuit Board. U.S. Patent No. 6,024,589, 15 February 2000.
3. Jung, H.S. Study for temperature rise on busbar of the switchgear and controlgear assemblies. *Korea Inst. Inf. Commun. Eng.* **2017**, *21*, 379–385.
4. Lee, Y.D.; Jeong, S.H. A design and implementation of busbar joint and temperature measurement system. *J. Korea Inst. Inf. Commun. Eng.* **2017**, *21*, 379–385. [CrossRef]
5. Kim, H.M.; Choi, J.Y. Study on the optimization of the fan position for cooling of the busbar of the enclosed switchboard. *Trans. Korean Soc. Mech. Eng. B* **2018**, *42*, 9–16. [CrossRef]

6. Kim, J.W.; Park, J.Y.; Sohn, J.M.; Ahn, K.Y. A study on thermal characteristics for D.C. molded cased circuit breaker busbar. *Korean Inst. Electric. Eng.* **2014**, *11*, 252–254.
7. Hedia, H.; Henrotte, F.; Meys, B.; Dular, P.; Legros, W. Arrangement of phases and heating constraints in a busbar. *IEEE Trans. Magn.* **1999**, *35*, 1274–1277. [[CrossRef](#)]
8. Kim, C.K.; Park, Y.H.; Kim, J.Y. Busbar design of high power HVDC converter. *Trans. Korean Inst. Electr. Eng.* **2012**, *61*, 923–927. [[CrossRef](#)]
9. Fuentes, C.D.; Rojas, C.A.; Renaudineau, H.; Kouro, S.; Perez, M.A.; Meynard, T. Experimental validation of a single DC bus cascaded H-bridge multilevel inverter for multistring photovoltaic systems. *IEEE Trans. Ind. Electron.* **2017**, *64*, 930–934. [[CrossRef](#)]
10. Callegaro, A.D.; Guo, J.; Eull, M.; Danen, B.; Gibson, J.; Preindl, M.; Emadi, A. Bus bar design for high-power inverters. *IEEE Trans. Power Electron.* **2018**, *33*, 2354–2367. [[CrossRef](#)]
11. Wang, L.; Chiang, H.D. Toward online bus-bar splitting for increasing load margins to static stability limit. *IEEE Trans. Power Syst.* **2017**, *32*, 3715–3725. [[CrossRef](#)]
12. Geng, C.; He, F.; Zhang, J.; Hu, H. Partial stray inductance modeling and measuring of asymmetrical parallel branches on the bus-bar of electric vehicles. *Energies* **2017**, *10*, 1519. [[CrossRef](#)]
13. Junior, M.F.; Bezerra, U.H.; Leite, J.C.; Moya, R.J.L. Maintenance tools applied to electric generators to improve energy efficiency and power quality of thermoelectric power plants. *Energies* **2017**, *10*, 1091. [[CrossRef](#)]
14. Dawson, F.P.; Cao, M.; Jain, P.K. A simplified approach to calculating current distribution in paralleled power buses. *IEEE Trans. Magn.* **1990**, *2*, 971–974. [[CrossRef](#)]
15. Bottauscio, O.; Carpaneto, E.; Chiampi, M.; Chiarabaglio, D.; Panaitescu, I. Numerical and experimental evaluation of magnetic field generated by power busbar system. *IEE Proc.-Gener. Transm. Distrib.* **1996**, *143*, 455–460. [[CrossRef](#)]
16. Chiampi, M.; Chiarabaglio, D.; Tartaglia, M. A general approach for analyzing power busbars under a.c. conditions. *IEEE Trans. Magn.* **1993**, *29*, 2473–2475. [[CrossRef](#)]
17. Labridis, D.P.; Dokopoulos, P.S. Electromagnetic forces in three-phase rigid busbars with rectangular cross-sections. *IEEE Trans. Power Deliv.* **1996**, *11*, 793–800. [[CrossRef](#)]
18. Bottauscio, O.; Chiampi, M.; Chiarabaglio, D. Experimental validation of a numerical model of busbar systems. *IEE Proc. C* **1995**, *142*, 65–72. [[CrossRef](#)]
19. Hwang, C.C.; Chang, J.J.; Jiang, Y.H. Analysis of electromagnetic and thermal fields for a bus duct system. *Electr. Power Syst. Res.* **1998**, *45*, 39–45. [[CrossRef](#)]
20. Fominykh, Y.A.; Sokovishin, Y.A.; Osotov, V.N.; Maslennikov, D.S.; Konstantinov, A.G.; Parylis, M.E.; Greditor, A.M. Temperature distribution over the surface of rectangular busbars in electrical apparatus. *Elektrichestvo* **1992**, *4*, 53–56.
21. Schoft, S. Joint resistance depending on joint force of high current aluminum joint. In Proceedings of the 50th IEEE Holm Conference on Electrical Contacts and the 22nd International Conference on Electrical Contacts, Seattle, WA, USA, 23–23 September 2004; pp. 502–510.
22. Braunovic, M. Evaluation of different contact-aid compounds for aluminum-to-copper connections. In Proceedings of the 36th Annual Holm Conference on Electrical Contacts, Montreal, QC, Canada, 20–24 August 1990; pp. 509–517.
23. Schlegel, S.; Großmann, S.; Lobl, H.; Hoidis, M.; Kaltenborn, U.; Magier, T. Joint resistance of bolted copper-copper busbar joints depending on joint force at temperatures beyond 105 °C. In Proceedings of the Annual Holm Conference on Electrical Contacts, Charleston, SC, USA, 4–17 October 2010; pp. 444–451.
24. Chapman, D. *Copper for Busbars: Guidance for Design and Installation*; Copper Development Association: Hemphstead, HP, UK, 1954; pp. 25–27.

